Experimental Investigation into the Behaviour of Continuous Concrete beams Reinforced with Basalt FRP

Rabee Shamass [a], Bouchra Mahi [b], Katherine A. Cashell[c], Ikram Abarkan [d], Fadoua El-Khannoussi [b]

[a] Division of Civil and Building Services Engineering, School of the Built Environment and Architecture, London South Bank University, UK

[b] SCD Laboratory, Abdelmalek Essaadi University,Tetouan, Morocco

[c] Dept of Civil and Environmental Engineering, Brunel University London, UK

[d] Department of Physics, Faculty of Sciences, Abdelmalek Essaâdi University, Tetouan, Morocco

Abstract

The durability of reinforced concrete structures is an ongoing challenge for engineers, particularly in harsh environments such as industrial or marine settings. This paper is concerned with continuous concrete beams which are reinforced with basalt fibre reinforced polymer (BFRP) reinforcing bars, rather than traditional steel rebars, to improve the durability. Continuous concrete members are commonly used in bridges and carparks and therefore may be susceptible to corrosion by being a harsh environment or through exposure to de-icing salts. There are increasing levels of interest in structural solutions that offer durability as well as mechanical performance, and in this context, BFRP reinforcement can provide an effective, sustainable, and durable solution. This paper describes an experimental programme comprising four, two-span continuous reinforced concrete beams, containing BFRP rebars and stirrups. The test results are analysed in the paper, with particular focus given to the cracking behaviour, bending capacity, moment redistribution and deflections. The test results are compared with American and Canadian design codes. It is found that both design codes overestimate the cracking moment and sagging bending moment capacity but underestimate the deflections. Furthermore, this research found that BFRP RC continuous beams exhibited at least 20% moment redistribution. The findings from this research suggest that the RC continuous beams can be entirely reinforced with BFRP rebars and stirrups to achieve corrosion free concrete element.

Keywords: Basalt-fibre-reinforced-polymer (BFRP); durability; moment redistribution; reinforced concrete; continuous beam, moment capacity; sustainability; design guidance.

Introduction

This paper is concerned with the behaviour of continuous reinforced concrete beams, containing durable basalt fibre reinforced polymer (BFRP) rebars. Although a degree of cracking is expected to occur in reinforced concrete, excessive cracking and widening of existing cracks can pose major problems not only to the load-carrying capacity, but also in terms of deterioration of the reinforcement and the bond between the bars and the surrounding concrete. This, in turn, can shorten the service life of structures and increase the inspection and maintenance costs. For reinforced concrete (RC) infrastructure in harsh environments, such as near the coast or in some bridges, carparks and underground tanks, excessive cracking may reduce the structural durability by allowing water and aggressive chemicals to ingress, causing

corrosion of the reinforcing steel. Corrosion reduces the cross-sectional area of the reinforcing steel thus resulting in a lower load-bearing capacity of the RC member and possible premature failure. Studies have shown that under excessive corrosion, the reinforcing steel suffers a significant loss of ductility, reduction in yield and ultimate strength, and deterioration in bond properties [1, 2]. Clearly, these issues endanger the safety and serviceability of reinforced concrete structures and also have negative economic, environmental and social consequences.

There are a number of different ways of dealing with the corrosion problem in RC structures, most of which are quite expensive. These include galvanized or dual-coated zinc and epoxy reinforcing steel [3] and also the installation of cathodic protection. However, these methods may not provide a sufficient solution to the steel reinforcement corrosion problem, and also increase the material usage overall. The use of fibre reinforced polymer (FRP) rebars in lieu of traditional steel reinforcing bars can provide an effective and alternative solution. FRP's are generally non-corrodible, and also possess other favourable qualities such as high tensile strength and low weight. They also have a relatively low modulus of elasticity compared with carbon steel, a linear stress-strain relationship until rupture, and low transverse strength.

There are many different types of FRP reinforcement including glass (GFRP) and carbon (CFRP) composites, which are quite common, as well as a newer type made from basalt fibres, BFRP. BFRP is produced from melting crushed volcanic rock, to create basalt fibres (BFs). BFRP is characterized by its excellent corrosion and thermal resistance, light weight (one-third of the weight of steel for example) and high strength, in comparison to steel and GFRP. In addition, BFRP is a highly sustainable, non-polluting, non-hazardous green construction material which has excellent resistance to deterioration in an alkaline environment compared with other types of FRPs [4]. The production process of BFs is simpler and requires less energy compared with the production of glass fibres [5] and they are readily recyclable unlike GFRP or CFRP which require high temperatures and/or chemicals to be recycled [6].

This paper proceeds with an overview of the existing research and design information relevant to the behaviour of continuous RC beams with BFRP reinforcement. Although these have not previously been studied explicitly, there have been other studies on members with GFRP or CFRP rebars, as well as single-span beams with BFRP reinforcement. A test program comprising four, two-span continuous beams with BFRP rebars and stirrups is described. A discussion of the results and observations is given and the results are compared with the guidance provided in available international design codes.

2. RC structural members with FRP reinforcement – A review

The current paper is concerned with the behaviour of continuous RC beams with BFRP reinforcement. In this section, existing relevant research on RC beams, single-span and continuous, with FRP rebars is presented. Generally, there is significantly more research data available on members with GFRP or CFRP compared with BFRP reinforcement, as these are more established materials in structural applications. It has been found that GFRP and/or CFRP can be effectively used as both flexural and shear reinforcement in RC beams [7-13]. Reinforced concrete beams containing CFRP, GFRP or BFRP rebars generally fail either by

concrete crushing or rupture of the reinforcement, depending on the reinforcement ratio, similarly to traditional carbon steel RC members. In general, there are relatively high levels of deformation before failure for all FRP RC beams. In terms of the cracking behaviour, the behaviour is similar for RC beams reinforced with either CFRP, GFRP or BFRP in that vertical cracks form initially in the pure bending zone then, at higher loads, more cracks develop along the beam length and these tend to incline towards the central (high moment) region. It was shown that RC beams with GFRP or BFRP rebars are generally less stiff after the initial cracks have formed compared with similar members with CFRP reinforcement, owing to the greater modulus of elasticity of CFRP. Additionally, CFRP RC beams exhibited slightly higher carrying capacity compared with GFRP or BFRP RC beams.

The existing body of research into BFRP RC beams has focused on simply supported, single-span members. These have been shown to have greater flexural capacity compared with equivalent traditional RC beams (i.e. similar reinforcement ratio, geometry, and concrete strength), but also tend to deflect more and have a greater number of cracks develop owing to the lower modulus of elasticity of BFRP rebars relative to steel rebars [14-16]. Research studies have concluded that the shear behaviour of BFRP RC simply supported beams is affected by both the flexural and the shear reinforcement ratio [17], the shear span-to-depth ratio [18], the depth of the beams and also the concrete strength [19,20]. For members with a low reinforcement ratio, BFRP RC beams exhibit a greater number of flexural and shear cracks compared with traditional carbon steel reinforced concrete members [21].

As stated before, the current paper is concerned with the behaviour of continuous BFRP reinforced concrete members. Continuous beams are common in structures such as carparks and bridges, both of which can be vulnerable to corrosion owing to the use of de-icing salts and possibly the local environment. Researchers have studied continuous beams with GFRP or CFRP reinforcement, and a brief discussion on the relevant findings is included herein. It was shown that continuous RC beams with GFRP or CFRP reinforcement have sufficient capacity and ductility to redistribute bending moments over the intermediate support [22]. Similarly, Habeeb and Ashour [23] tested continuous RC beams reinforced with GFRP longitudinal bars and steel stirrups and found that the GFRP RC beams exhibited greater deflections and crack widths compared with equivalent traditional RC beams. Ashour and Habeeb [24] tested three continuous beams reinforced with longitudinal CFRP and steel stirrups and found that increasing the CFRP reinforcement ratio at the midspan enhanced the load capacity and also provided a reasonable level of control on the deflections.

It is noteworthy that in reinforced concrete construction, the steel stirrups are often the most vulnerable reinforcement in terms of exposure to an aggressive environment since they are the outmost reinforcement layer. Research studies found that high levels of chloride-induced corrosion lead to a reduction in the cross-sectional area of carbon steel stirrups and can also result in corrosion-induced cracking of the concrete cover to the stirrups [25]. This may result in a significant reduction in the ductility, shear strength and stiffness of the members as well as a loss in bond between the stirrups and the concrete, and can result in sudden shear failure [25, 26].

Rahman and El-Salakawy [27] reported the experimental results from tests on three continuous RC beams with a T-shaped cross-section and reinforced with GFRP rebars and stirrups. It was concluded that beams with a relatively low spacing between adjacent stirrups had a greater percentage of moment redistribution from the hogging to sagging moment regions compared with members with greater distances between the stirrups, as well as a greater ultimate capacity. Basa et al. [28] conducted tests on seven continuous beams with different arrangements of GFRP longitudinal and transversal reinforcement in the midspan region and at the intermediate support. The results indicated that the continuous GFRP reinforced beams were able to redistribute the bending moments at the internal support without causing a reduction of the load bearing capacity of the beams. The degree of moment redistribution achieved was dependent on the stiffness of the critical sections at the midspan and interior support. The experimental results were also compared to existing code provisions, showing that the American ACI 440.1R-06 [29] standard provides a reasonable estimate of the failure load for continuous beams with GFRP reinforcement while the Canadian CSA S806-12 [30] code slightly overestimates the failure load. On the other hand, both standards underestimate the level of deflection for continuous beams with GFRP reinforcement. Mahmoud and El-Salakawy [31] conducted an experimental investigation specifically into the shear behaviour of continuous RC beams reinforced with GFRP rebars and stirrups. It was concluded that the moment redistribution at the internal support was equal or higher than the design value of 20%, enabling the beam to support greater loads than would otherwise have occurred. In another research study, Mahmoud and El-Salakawy [32] examined six continuous beams reinforced with GFRP rebars and stirrups and, similar to the other studies, found that the beams failed in shear near the internal support after significant levels of moment redistribution occurred.

In conclusion to this section, and following a detailed review of the available and relevant literature, it is concluded that the behaviour of continuous concrete beams reinforced with BFRP rebars and stirrups has not yet been investigated in any detail in the available literature. The behaviour of these members is important, and likely to become increasingly so as the importance for durability and sustainability in construction continues to intensify.

3. Experimental programme

3.1. Test specimens

A total of four reinforced concrete beams continuous over two spans were cast and tested at the Structures Laboratory in the Division of Civil Engineering at London South Bank University. The overall length of the beams was 4.2 m and they had a rectangular cross-section which was 200 mm in width and 270 mm in overall depth. The beams were continuously supported over two clear spans, each equal to 1.9 m, and were subjected to a single point load at the middle of each span. The geometric and reinforcement details of the beams are given in Table 1 and also illustrated in Fig. 1. In this table, f_c is the compressive strength of the concrete and ρ is the reinforcement ratio.

The beams were designed such that four different reinforcement ratios were examined in the top region at the interior support and in the bottom region of the main spans. All of the beams

included sand-coated BFRP shear stirrups, which were 8.5 mm in diameter and spaced at 100 mm intervals along the beam length, corresponding to a 0.57% shear reinforcement ratio. The beams were also reinforced with two helically-wrapped BFRP rebars in the longitudinal direction, as shown in Fig. 1. An image of the reinforcement arrangement prior to casting is presented in the Fig. 2. The four beams have unique names (i.e. B-0.24-0.61, B-0.24-0.24, B-0.61-0.24 and B-0.61-0.61) where the first letter indicates that the specimens are beams (B), the next number (0.24 or 0.61) refers to ρ_f for the top longitudinal reinforcement and the final number (again, 0.24 or 0.61) describes ρ_f for the bottom longitudinal reinforcement of the beam. For example, B-0.61-0.24 denotes a beam with a reinforcement ratio of 0.61% and 0.24% for the top and bottom longitudinal reinforcement, respectively, as seen in the Table 1.
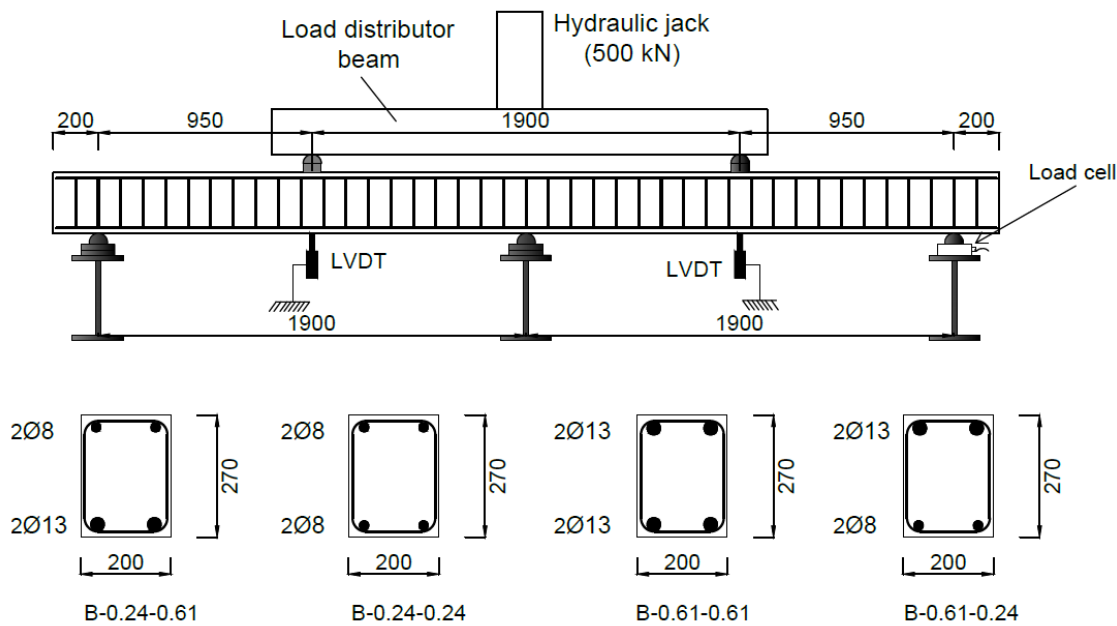
Figure 1: Experimental setup and cross-sectional details of tested beams (all dimensions in mm)

There are several international design codes for glass, carbon, glass, and aramid FRP RC structures, including the American ACI 440.1R-06 code [29] and the Canadian CSA S806-12 standard [30]; however, specific guidance for BFRP RC structures is not included in any standard, mainly owing to a lack of available performance data. Recent research into the flexural behaviour of simply supported BFRP RC beams proposed that the American and Canadian codes could be safely applied for BFRP RC single-span beams [14]. In the current test programme, all of the beams were designed to avoid shear failure and assumed no moment redistribution would occur. Accordingly, the design shear capacities were higher that the design flexural capacities in all cases, based on the American ACI 440.1R-06 design rules [29].

Figure 2: BFRP reinforcement arrangement

Table 1: Concrete strength and reinforcement details of the beams

Beam	f_c (MPa)	BFRP Flexural reinforcement					BFRP stirrups	
			Bars	ρ_f (%)	$\rho_f/\rho_{b,ACI}$	$\rho_f/\rho_{b,CSA}$	Bar size	Spacing (mm)
B-0.61-0.24	18.4	top	2 Ø13.4	0.61	4.72	3.84	8.5	100
		bottom	2 Ø8.4	0.24	2.12	1.73		
B-0.61-0.61	18.2	top	2 Ø13.4	0.61	4.87	3.95	8.5	100
		bottom	2 Ø13.4	0.61	4.87	3.95		
B-0.24-0.24	25	top	2 Ø8.4	0.24	1.44	1.21	8.5	100
		bottom	2 Ø8.4	0.24	1.44	1.21		
B-0.24-0.61	26	top	2 Ø8.4	0.24	1.38	1.16	8.5	100
		bottom	2 Ø13.4	0.61	3.08	2.59		

3.2. Material properties

The beams were cast using ready-mixed concrete with a target 28-day concrete compressive strength of 20 MPa. The maximum aggregate size was 10 mm, and the measured slump was 220 mm. Six standard cubes were cast from each concrete batch to determine the compressive strength of concrete f_c on the day of beam testing. After concrete casting, the beams and cubes were covered with plastic sheets until the day of testing. The average compressive strength f_c of each batch of concrete on the day of beam testing is given in Table 1. Fig. 3(a) shows the moulds for the beam specimens with the BFRP reinforcement cage in position and Fig. 3(b) illustrates the concrete beam samples three days after casting.

(a)   (b)

Figure 3: concrete beams before and after costing

The shear reinforcement comprised sand-coated BFRP bars with a nominal diameter Ø of 8.5 mm, an external bend radius of 32 mm, and an average external width and height of 165 mm and 219 mm, respectively (see Fig. 4). The mechanical properties of the straight portion these bars were provided by the manufacturer, and are presented in Table 2, including the tensile strength f_u, ultimate strain ε_u and elastic modulus E_f. The nominal diameters of each bar type are also given which were determined in accordance with ISO 10406-1 [33] based on at least five representative samples. For the longitudinal reinforcement, helically-wrapped BFRP rebars were employed which had a nominal diameter Ø of either 13.4 mm or 8.4 mm, and the mechanical properties are also given in Table 2. Fig. 4 presents a photographic image of the BFRP rebars used in the current study including (a) the stirrups and (b) the straight longitudinal bars.

Table 2: Properties of the BFRP bars and stirrups

Bar type	Nominal diameter Ø (mm)	Tensile strength f_u (MPa)	Elastic modulus E_f (GPa)	Ultimate strain ε_u (%)
Stirrups	8.5	1151	47.8	2.4
Straight rebar	8.4	1018	44.5	2.3
	13.4	950	45.3	2.1
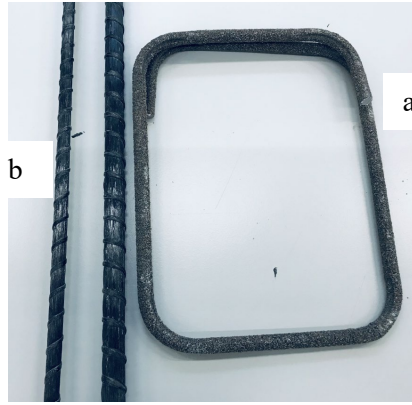
Figure 4: Basalt FRP samples including (a) a sand-coated stirrups and (b) helically-wrapped bars

2.3. Instrumentation and testing procedure

The testing was conducted in the Structures Laboratory in the Division of Civil Engineering at London South Bank University. All beams were painted white before testing to facilitate a close visual analysis of the crack development. The exterior and interior supports were levelled before placing the beams under the hydraulic loading jack. A monotonic concentrated load was applied to a rigid steel spreader box beam, as shown in Fig. 1, which delivered two equal point loads (P/2, where P is the total applied load from the loading jack) to the middle of each span. The beams were loaded in displacement-control at a rate of 1.5 mm/min until failure occurred. The vertical deflection at the midpoints of each span of each beam was recorded using linear variable differential transducers (LVDT). Each beam was instrumented with a load cell to measure the reactions at the exterior supports. An automatic-data acquisition system was used to monitor the applied loads and deflections. The development of cracks and their distributions along the length of the beams were closely monitored and manually recorded, during the tests. Once the first crack was visible during each test, the loading was paused and the crack was marked on the specimen. The tests were then re-started and the cracks were marked at 20 kN intervals.

3. Test results and discussion

This section presents the main observations and discussion of the test results. There are several important structural performance measures for reinforced concrete continuous beams and each is discussed hereafter with reference to the relevant international design codes, namely ACI 440.1R-06 [29] and CSA S806-12 [30]. The performance measures discussed are (1) load-deflection response, (2) crack propagation and failure mode, (3) cracking moment, (4) ultimate capacity, (5) moment redistribution and (6) deflections.

3.1. Load-deflection behaviour

Fig. 5 presents the load *versus* deflection response for all of the tested RC beams; the deflections presented are those that were measured at the middle of the left-hand span. The results are also presented in tabular form in Table 3 where P_{cr} and M_{cr} are the load and moment at first cracking, respectively, P_u is the ultimate load and δ_u is the deflection corresponding to P_u. Initially, at low levels of load, beams B-0.61-0.24, B-0.61-0.61 and B-

0.24-0.61 behaved very similarly to each other, and experienced first cracking at comparable load levels. Thereafter, the load increased steadily for all beams until the ultimate load was reached. This was then followed by a brittle failure resulting in a sudden drop in the load-carrying capacity.

Furthermore, beams with the same reinforcement ratios in the sagging moment regions (e.g. B-0.24-0.61 and B-0.61-0.61) exhibited similar stiffness responses prior to the ultimate load. Furthermore, beams with the relatively higher reinforcement ratio in the sagging moment region (B-0.24-0.61 and B-0.61-0.61) exhibited a stiffer response, regardless of the reinforcement ratio in the hogging moment region; this resulted in lower deflections. With reference to the data presented in Fig. 5 and Table 3, it is noted that beams with a similar ρ in the hogging moment region achieved similar levels of deflection at the ultimate load (δ_u) and, as ρ in the hogging moment region increased, δ_u also decreased. For example, δ_u for beam B-0.61-0.61 was 26% lower than for beam B-0.24-0.61 but was quite similar to the value observed for B-0.61-0.24.
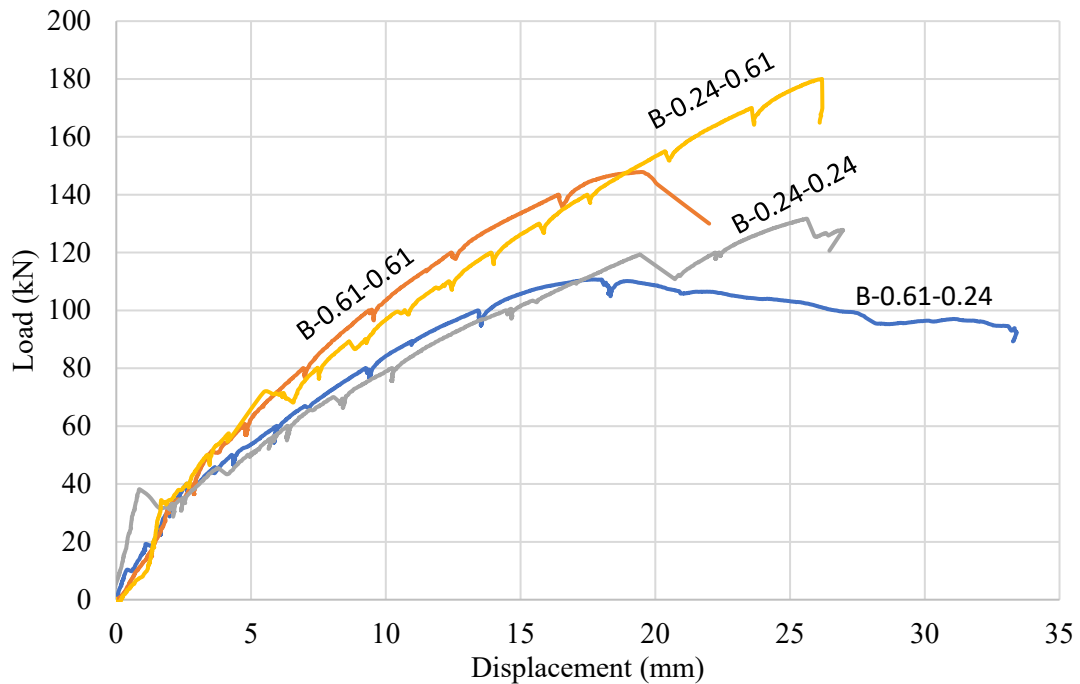
Figure 5: Load-deflection response for the tested beams

3.2. Crack propagation and failure mode

As stated before, a careful examination of the propagation of cracks was conducted during each of the tests. To illustrate the typical pattern of crack development, beam B-0.61-0.61 is selected herein and Fig. 6 presents a schematic view of the various cracks that developed at (a) P=40 kN, where P is the total applied load, (b) P=60kN, (c) P=80 kN, (d) P=120 kN, and (e) P_u=147.9 kN (ultimate load). This specimen was selected for illustrative purposes and similar observations were found for the other test specimens. The first crack generally initiated either at the midspan on one side of the beam, on the lower surface, or at the top of the section near the interior support, and then propagated vertically towards the compression

zone. As the load increased, new flexural cracks continued to form in all regions of the beams while the existing cracks widened and propagated towards the compression zone up. After about 53% of the ultimate load, the number of new cracks forming decreased. As the loading was increased further, the cracks started to propagate diagonally towards either the interior support or the loading points because of the combination of flexural and shear stresses.

Fig. 7 shows a schematic of the crack pattern at P_u for each of the 4 beams, where the failure crack is highlighted. It is observed that failure of B-0.61-0.24, B-0.61-0.61 and B-0.24-0.61 occurred due to concrete crushing failure in combination with a diagonal shear crack at one side of the interior support while beam B-0.24-0.24 failed due to concrete crushing failure in combination with a diagonal shear crack near the point of loading on the right hand span of the beam. All longitudinal BFRP rebars (either in tension or compression) failed by a loss in dowel action. It was noted that the stirrups were not ruptured at failure. It was observed during the tests that at P_u, the inclination of the diagonal cracks near the interior support was higher than those formed in the midspan region. Furthermore, the spacing between the main cracks was between 150-200 mm, which is larger than the spacing between adjacent stirrups. With reference to Fig. 7, it is clear that the beam with the lowest reinforcement ratio (i.e. B-0.24-0.24 in Fig. 7(c)), had a quite different crack pattern at failure compared with the other beams. There was only one crack at the interior support and this propagated vertically without the formation of any diagonal cracks while a relatively small number of cracks developed in the sagging moment region and these tended to propagate diagonally towards the point of load application.

The angle of inclination θ of the crack at which failure occurred in beams B-0.61-0.24, B-0.61-0.61, B-0.24-0.24 and B-0.24-0.61 was 48°, 49°, 60°, and 59° to the horizontal axis, respectively. The average angle of inclination was 54°, which is in good agreement with the observation by Mohamoud and El-Salakawy [31] for continuous RC beams reinforced with GFRP (53°).
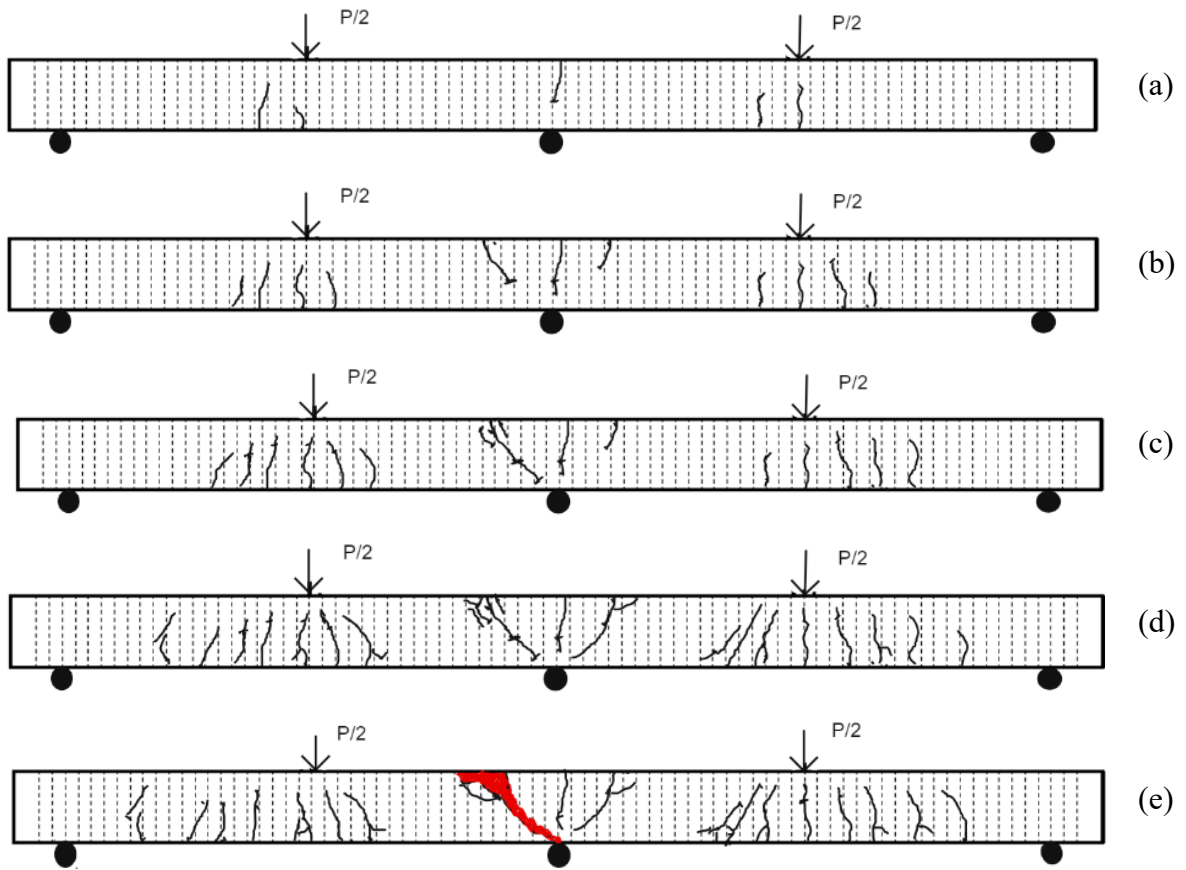
Figure 6: Crack patterns and propagation for the beam B-0.61-0.61 at P equal to (a) 40 kN; (b) 60 kN; (c) 80 kN; (d) 120 kN; and (e) 148 kN (P_u)
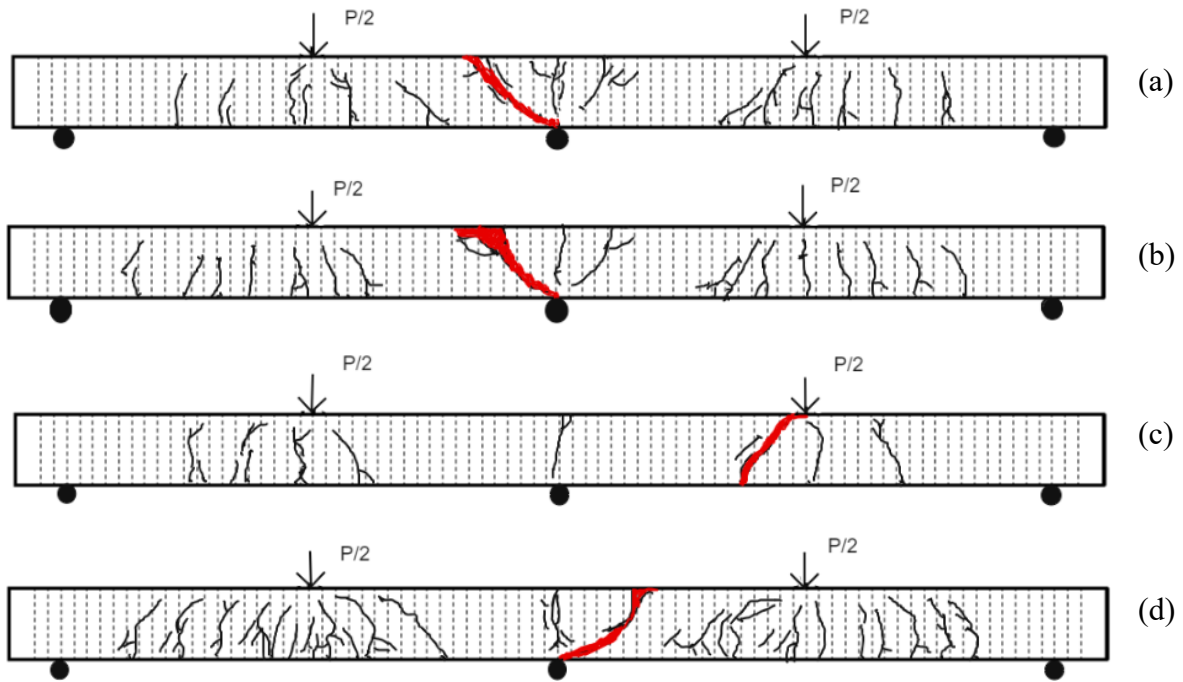
Figure 7: Cracking pattern at failure for the beams (a) B-0.61-0.24; (b) B-0.61-0.61; (c) B-0.24-0.24; and (d) B-0.24-0.61.

3.3. Cracking moments

The cracking load P_{cr} corresponding to the development of the first visible crack for each beam was recorded during testing and the cracking moment (M_{cr}) was then calculated; the results are presented in Table 3. The location of the first crack is also given in the table (either at the midspan or near the interior support) as well as the distance between the first crack and the left exterior support for each beam. P_{cr} ranged from between 7% to 24% of P_u for the examined beams. It is noteworthy that as the reinforcement ratio in the sagging moment region increased, the cracking moment also increased. For instance, the cracking moment for the beams B-0.61-0.61 and B-0.24-0.61 were 59% and 58% higher than for B-0.61-0.24 and B-0.24-0.24, respectively.

In addition to the experimental cracking moments observed during the tests, Table 3 also presents the ratio of the theoretical cracking moments determined in accordance with the ACI design standard $M_{cr, ACI}$ [29] and the Canadian code $M_{cr, CSA}$ [30] to M_{cr} from the experiments. The theoretical cracking moment ($M_{cr,ACI}$ and $M_{cr,CSA}$) is determined as:

$$M_{cr,ACI} = M_{cr,CSA} = \frac{f_r I_g}{y_t}$$

(1)

where f_r is the modulus of rupture of the concrete, I_g is the gross moment of inertia of the section and y_t is the vertical distance between the extreme tension fiber and the neutral axis, and can be taken as half of the beam's depth. From the American [29] and Canadian [30] design codes, f_r is calculated using Eqs. 2 and 3, respectively:

$$f_{r,ACI} = 0.62\sqrt{f_c} \tag{2}$$

$$f_{r,CAN} = 0.6\sqrt{f_c} \tag{3}$$

With reference to the data presented in Table 3, it is observed that both design codes tend to overestimate the cracking moment for all of the tested beams. The average predicted-to-experimental cracking moment based on ACI and CSA design codes are 1.87 and 1.81, respectively. Similar observations were found for BFRP RC simply supported beams tested by Shamass and Cashell [14] and Elgabbas et al. [15].

Duic et al. [21] tested simply supported beams reinforced with steel or BFRP longitudinal rebars and stirrups and found that the cracking moments from the steel RC beam were 30-40% higher than those observed for the BFRP RC beams. Shamass and Cashell [14] found that the type of BFRP rebar (sand-coated or ribbed) and the type of reinforcement (BFRP and steel) affected the cracking moment values for simply supported RC beams. It was also found that the cracking moment for steel RC beams is between 30-80% higher than those observed for BFRP RC beams. Therefore, it has been shown that the reinforcement ratio, rebar stiffness and surface roughness all affect the cracking moment values for RC beams, although these parameters are not explicitly included in the design standards. A further issue that contributes to the likely overestimation of the calculated cracking moment is that codified expressions do not allow for the effect of restrained shrinkage of the concrete, which tends to reduce the experimental cracking moment. It is noteworthy that as the elastic modulus of BFRP rebars is comparatively low compared with traditional steel reinforcement, there is less restrained shrinkage also.

Table 3: Experimental and theoretical cracking moment values for the test specimens

Specimen	Experiment				Location of the first crack		Predicted-to-tested	
	P_{cr} (kN)	P_u (kN)	δ_u (mm)	M_{cr} (Kn.m)	Midspan /interior support	Distance (m)	$\dfrac{M_{cr,ACI}}{M_{cr}}$	$\dfrac{M_{cr,CSA}}{M_{cr}}$
B-0.61-0.24	16.5	110.7	17.8	1.96	Midspan	1.10	2.75	2.84
B-0.61-0.61	16.8	147.9	19.2	3.11	Midspan	0.95	1.70	1.76
B-0.24-0.24	32	131.7	25.8	3.86	interior support	1.90	1.70	1.75
B-0.24-0.61	11.8	180	26.1	6.09	Midspan	1.025	1.10	1.13
Average							1.87	1.81

3.4. Failure loads and moments for the tested beams

The ultimate load achieved in each of the tests P_u is presented in Table 3. It is observed that the failure load was greater for beams with a higher reinforcement ratio in the sagging moment region. The failure loads for B-0.61-0.61 and B-0.24-0.61 were higher than for B-0.61-0.24 and B-0.24-0.24 by 34% and 37%, respectively. Even though the top reinforcement ratio of B-0.24-0.61 was about 40% of the corresponding value for B-0.61-0.61, B-0.24-0.61 reached a load which was around 21% greater than B-0.61-0.61. Similarly, B-0.24-0.24 reached a load which was around 19% greater than B-0.61-0.24. Overall, B-0.61-0.24 had the lowest load capacity while B-0.24-0.61 had the greatest load capacity of the examined beams. This is because the moments in the sagging moment regions of B-0.61-0.24 were redistributed to the hogging moment region near the interior support, resulting in a reduction in the load-bearing capacity. On the other hand, moment redistribution also occurred in B-0.24-0.61 but from the hogging moment region to the sagging moment regions, thus enhancing the load bearing capacity of this beam. This is discussed in greater detail in the section 3.4 of this paper. The shear stresses in the sections also have an influence on the ultimate load capacity of the tested beams. In the uncracked concrete zone, high shear stresses exist jointly with compressive stresses, resulting in a biaxial compression-tension stress state which reduces the resistance of the compressed zone and, therefore the ultimate capacity.

The flexural design for FRP RC is based on the principles of equilibrium, strain compatibility, and the stress-strain relationship of FRP and concrete. If the FRP reinforcement ratio (ρ_f) is higher that the balanced reinforcement ration (ρ_b) then the section fails by concrete crushing. On the other hand, when the FRP reinforcement ratio (ρ_f) is higher that the balanced reinforcement ration (ρ_b) then the section fails by FRP rupture. The balanced reinforcement ration ρ_b according to American [29] and Canadian [30] design standards are calculated using Eqs. 4a and 4b, respectively:

$$\rho_{b,ACI} = 0.85\beta_1 \frac{\varepsilon_{cu}}{\varepsilon_{cu} + \varepsilon_u} \frac{f_c}{f_u}$$

$$\text{where: } \beta_1 = 0.85 - 0.05\frac{f_c - 27.6}{6.9}$$

(4a)

$$\rho_{b,CSA} = \alpha_1 \beta_1 \frac{\varepsilon_{cu}}{\varepsilon_{cu} + \varepsilon_u} \frac{f_c}{f_u}$$

$$\text{where: } \alpha_1 = 0.97 - 0.0025 f_c \geq 0.67; \quad \beta_1 = 0.85 - 0.0015 f_c \geq 0.67$$

(4b)

In these expressions, f_c is the compressive strength of concrete, ε_{cu} is the ultimate compressive strain of concrete (0.003 for the American guide and 0.0035 for the Canadian).

All of the BFRP RC beams in the current programme were designed to fail by concrete crushing and so the BFRP reinforcement ratio was greater than the balanced reinforcement ratio according to American and Canadian design standards, as seen in the Table 1. Both the American [29] and Canadian [30] design standards contain expressions for calculating the

bending moment capacity of the FRP reinforced beams when $\rho_f > \rho_b$; these procedures are given in Table 4 for $M_{u,ACI}$ and $M_{u,CSA}$, respectively. For these expressions, b and d are the width and depth of the cross section, respectively; A_f is the total cross-sectional area (in mm^2) of the longitudinal bars, respectively; E_f is the elastic modulus of the longitudinal bars; and f_f is the stress in the BFRP reinforcing bars.

Table 4: bending moment capacity design provisions using ACI and CSA

ACI 440.1R-06 [29]	$$M_{u,ACI} = \rho_f f_f \left(1 - 0.59 \frac{\rho_f f_f}{f_c}\right) bd^2$$ $$f_f = \left(\sqrt{\frac{(E_f \varepsilon_{cu})^2}{4} + \frac{0.85 \beta_1 f_c}{\rho_f} E_f \varepsilon_{cu}} - 0.5 E_f \varepsilon_{cu}\right) \le f_u$$ $$\rho_f = \frac{A_f}{bd} \quad, \quad \beta_1 = 0.85 - 0.05 \frac{f_c - 27.6}{6.9}$$
CSA-S806-12 [30]	$$M_{u,CSA} = \alpha_1 \beta_1 cb \left(d - \frac{\beta_1 c}{2}\right)$$ $$c = \frac{\rho_f f_f}{\alpha_1 f_c \beta_1} d$$ $$f_f = \left(\sqrt{\frac{(E_f \varepsilon_{cu})^2}{4} + \frac{\alpha_1 \beta_1 f_c}{\rho_f} E_f \varepsilon_{cu}} - 0.5 E_f \varepsilon_{cu}\right) \le f_u$$ $$\alpha_1 = 0.97 - 0.0025 f_c \ge 0.67$$ $$\beta_1 = 0.85 - 0.0015 f_c \ge 0.67$$

The experimental failure moments at the midspan and interior support are calculated from the measured end support reaction and midspan point load at the failure of each beam. The predicted-to-experimental failure moments ratios at the midspan (sagging moment) and interior support (hogging moment) sections are presented in Table 5 for each of the tested beams. It is observed that the Canadian design approach provides less conservative predictions of the hogging bending moment capacity compared with those predicted by the American design approach with the tested value being greater than the design value in all

cases. The average predicted-to-experimental hogging moment for all beams is 0.87 and 0.95 for the American and Canadian codes, respectively.

The failure moment in the sagging moment regions of the BFRP RC beams is, however, overestimated by both the American and the Canadian design standards. This might be because, at failure, the concrete crushing strain was reached at the interior support earlier than at the midspan and therefore, the design hogging moment capacities are more comparable with the experimental predictions. The differences in the bending moment predictions given by the ACI 440.1R-06 [29] and Canadian CSA S806-02 [30] are related to the assumed height of the compressive rectangular stress block in the concrete and the assumed ultimate concrete strain which is 0.003 for the American code and 0.0035 for the Canadian code.

Table 5: Experimental and theoretical bending moment values for the test specimens

Beam	Experimental bending moment M_{Exp} (kN.m)		ACI 440.1R-06 [29] $M_{u,ACI}$ (kN.m)				CSA S806-02 [30] $M_{u,CSA}$ (kN.m)			
	Sagging	Hogging	Sagging	$\dfrac{M_{u,ACI}}{M_{Exp}}$	Hogging	$\dfrac{M_{u,ACI}}{M_{Exp}}$	Sagging	$\dfrac{M_{u,CSA}}{M_{Exp}}$	Hogging	$\dfrac{M_{u,CSA}}{M_{Exp}}$
B-0.61-0.24	13	26.5	16.3	1.25	23.4	0.88	18.0	1.38	25.6	0.97
B-0.61-0.61	22	26.3	23.0	1.04	23.0	0.87	25.2	1.14	25.2	0.96
B-0.24-0.24	19.5	23.6	20.3	1.04	20.3	0.86	22.1	1.13	22.1	0.94
B-0.24-0.61	30.8	23.9	30.4	0.99	20.8	0.87	32.8	1.07	22.6	0.95
Average				1.08		0.87		1.18		0.95

3.5. Reactions and moment redistribution

Moment redistribution occurs in continuous RC beams owing to the nonlinear behaviour of concrete, which is manifested in the concrete cracking as well as the nonlinear stress-strain behaviour of the concrete subjected to high levels of stress. Fig. 8 compares the measured end support reaction values with the total applied load for the tested beams. To assess the amount of load redistribution of each beam, the end support reaction obtained from an elastic analysis, assuming a uniform flexural stiffness throughout the entire beam, is also plotted. With reference to Fig. 8, in the early stages of loading before the concrete cracked, the measured and elastic support reactions were very close due to the linear elastic behaviour of the concrete and BFRP. After cracking occurred, the measured end support reaction for B-0.24-0.61 was larger than the elastic reaction, indicating that some of the load was redistributed from the hogging moment region (i.e. the interior support) to the sagging moment regions (i.e. middle of both spans) due to the higher stiffness at the midspan. The axial stiffness of the tensile reinforcement in the midspan regions was 2.54 times the equivalent value at the interior support. On the other hand, it is noteworthy that B-0.61-0.24 had a lower measured end support reaction compared with the reaction determined from an

elastic analysis, and also demonstrated the opposite moment redistribution pattern (i.e. load was redistributed from the midspan to the interior support, rather than vice versa) due to the reverse reinforcement configuration, as discussed before. When the axial stiffness of the tensile reinforcement in the sagging moment region and hogging moment regions were similar, as was the case for the beams B-0.24-0.24 and B-0.61-0.61, the measured end support reactions were shown to have been very close to those obtained from an elastic analysis.
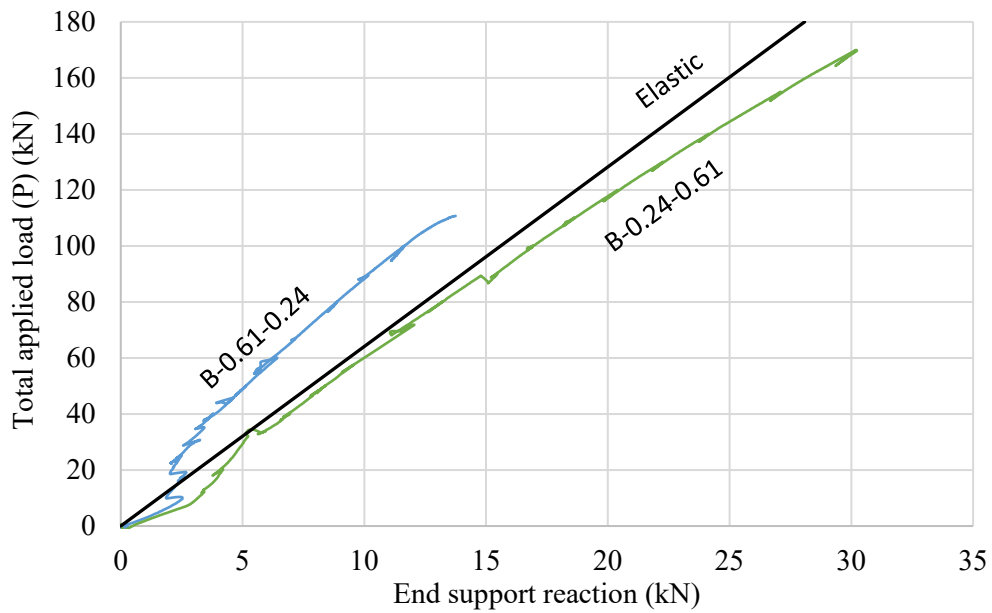
(a)
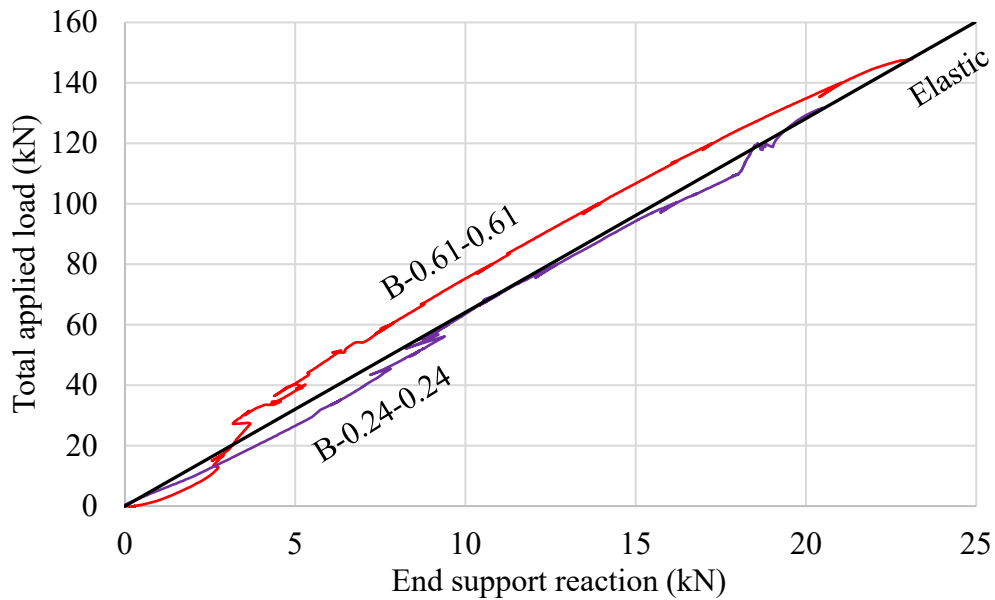
(b)

Figure 8: Applied load versus end-support reactions for the beams (a) B-0.61-0.24 and B-0.24-0.61 and (b) B-0.61-0.61 and B-0.24-0.24

Table 6 presents the experimental bending moment at failure (M_{Exp}) at both the midspan and the interior support obtained using the measured end support reactions and the applied loads, as well as the corresponding bending moments calculated from an elastic analysis (M_e). The elastic bending moment at the interior support (i.e. a hogging moment) is determined as $0.188(P_u/2)L$ and the bending moment at the midspan is obtained as $0.156(P_u/2)L$, where L is the span and P_u is the experimental ultimate load. If M_u is the ultimate moment at failure, the amount of moment redistribution (%) is determined as:

$$\text{Moment redistribution (\%)} = \frac{M_u - M_e}{M_e} \times 100 \qquad (5)$$

The data presented in Table 6 indicates that the experimentally calculated bending moments were quite different from those obtained from a linear elastic analysis at the failure load for beams B-0.24-0.61 and B-0.61-0.24 whilst for beams B-0.24-0.24 and B-0.61-0.61, the experimental and theoretical values were similar. The amount of moment redistribution in the hogging moment regions was always greater than that in the sagging moment sections for the tested BFRP continuous beams since the moment redistributes between the hogging moment region and both sagging moment regions. For beam B-0.61-0.24, redistribution of the bending moments from the midspan sections to the interior support did occur resulting in the lowest load bearing capacity of all of the examined members. On the other hand, for beam B-0.24-0.61, redistribution of bending moments also occurred but from the hogging moment section to the sagging moment regions, resulting in this continuous beam having the highest load capacity of the examined members. The beams with similar reinforcement ratios both in the midspans and at the interior support (i.e. B-0.24-0.24 and B-0.61-0.61) showed an almost negligible level of bending moment redistribution.

Beam B-0.61-0.24 exhibited the highest amount of experimental moment redistribution at the midspan (20.6%) and at the interior support (34.1%) of the examined members. This indicates that although the BFRP exhibited a linear-elastic stress-strain relationship up to failure without any clear yield point, the BFRP RC continuous beams nevertheless demonstrated an ability to redistribute bending moments after cracking of the concrete section. Moment redistribution can occur in BFRP reinforced members, depending on the relative reinforcement ratios in the hogging and sagging bending moment regions. Table 6 indicates the theoretical moment redistribution based on the theoretical moment capacity determined from ACI 440.1R-06 [29]. It is noteworthy that the members have sufficient ductility to allow for plastic deformation and therefore redistribution of moments. Indeed the theoretical moment redistribution at the interior support for B-0.24-0.61 was higher compared with the corresponding experimental value whilst it was lower for B-0.61-0.24.

Table 6: Bending moments and moment redistribution at failure

Beam	Experimental bending moment M_{Exp} (kNm)		Elastic bending moment M_e (kNm)		Experimental Moment redistribution %		Theoretical moment redistribution %	
	Sagging moment region (midspan)	Hogging moment region (interior support)	Sagging moment region (midspan)	Hogging moment region (interior support)	Sagging moment region (midspan)	Hogging moment region (interior support)	Sagging moment region (midspan)	Hogging moment region (interior support)
B-0.61-0.24	13.0	26.5	16.4	19.8	-20.6	34.1	-0.6	18.4
B-0.61-0.61	22.0	26.3	21.9	26.4	0.2	-0.3	4.9	-12.9
B-0.24-0.24	19.5	23.6	19.5	23.5	-0.2	0.4	4.0	13.7
B-0.24-0.61	30.8	23.9	26.7	32.1	15.5	-25.7	14	-35.3

3.6. Deflection behaviour

As stated before, the deflections at midspan of the beams were monitored and recorded during the tests on the continuous BFRP RC beams, so that the serviceability of these elements can be examined. Fig. 9 presents the load-midspan deflection responses from each of the test specimens, together with a number of theoretical approaches, which are described hereafter before a detailed analysis is presented.

3.6.1. ACI design standards

The maximum deflection at the midspan of a continuous beam δ subjected to concentrated loading P at the middle of the spans (L) can be calculated from Eq. 6:

$$\delta = \frac{7}{768}\frac{PL^3}{E_cI_e} \tag{6}$$

where E_c is the elastic modulus of the concrete according to ACI and I_e is the effective second moment of inertia of either the cracked or uncracked section. There are several methods for computing I_e. In the current work, the methods given in ACI 440.1R-06 [29], ACI 440.1R-15 [34] and the amendment proposed by Habeeb and Ashour [23] are explored.

The ACI 318-08 [35] code for structural steel reinforced concrete includes an expression for the determination of I_e, as originally proposed by Branson [36]. ACI 440.1R-06 [29] for FRP reinforced concrete included a modification factor β_d in the determination of I_e, as follows:

$$I_e = \left(\frac{M_{cr}}{M_a}\right)^3 \beta_d I_g + \left[1 - \left(\frac{M_{cr}}{M_a}\right)^3\right] I_{cr} \leq I_g \tag{7}$$

where $\beta_d = \frac{1}{5}\left(\frac{\rho_f}{\rho_b}\right) \leq 1$

In these expressions, M_{cr} is the cracking moment, M_a is the applied moment, and I_{cr} is the cracked moment of inertia for a reinforced concrete section, determined as:

$$I_{cr} = bd^3k^3/3 + nA_f\,d^2(1-k)^2 \tag{8}$$

n is the modular ratio between the BFRP reinforcement and the concrete.

$$k = \sqrt{2\rho_f n + (\rho_f n)^2} - \rho_f n \tag{9}$$

The more recent version of this code ACI 440.1R-15 [34] includes another formula for the calculation of I_e, given as:

$$I_e = \frac{I_{cr}}{1 - \gamma\left(\frac{M_{cr}}{M_a}\right)^2\left[1 - \frac{I_{cr}}{I_g}\right]} \leq I_g \tag{10}$$

where γ is an additional factor to account for the variation in stiffness along the length of the member, determined as:

$$\gamma = 1.72 - 0.72\left(\frac{M_{cr}}{M_a}\right) \tag{11}$$

In addition to these codified expressions, Habeeb and Ashour [23] investigated the specific behaviour of continuous GFRP RC beams, and suggested an amendment to the formulation for I_e as given in Eq. 7 to include a reduction factor $\gamma_G = 0.6$ as given in Eq. 13:

$$I_e = \left(\frac{M_{cr}}{M_a}\right)^3 \beta_d I_g + \left[1 - \left(\frac{M_{cr}}{M_a}\right)^3\right]\gamma_G I_{cr} \leq I_g \tag{12}$$

For continuous members, the effective moment of inertia should be calculated in both the hogging and sagging bending moment critical sections and the average value for beams with one continuous end can be obtained using the following formula [23]:

$$I_e = 0.85I_{em} + 0.15I_{ec} \tag{13}$$

where I_{em} and I_{ec} are the effective moment of inertia at the middle span section and at the interior support, respectively.

3.6.2. CSA S806-12 [30] design standard

The deflection at the midspan of a continuous, two-span RC beam with single point loads in the middle of each span can be determined as [28]:

$$\delta = \frac{P\,L^3}{48E_c I_{cr}}\left[\frac{5}{16} - \frac{15}{8}\left(1 - \frac{I_{cr}}{I_g}\right)\left(\frac{L_g}{L}\right)^3\right] \tag{14}$$

In this expression, E_c elastic modulus of concrete according to CSA, L_g is the distance from the edge support to the point where the applied moment is equal to the cracking moment.

3.6.3. Comparison with the beam test results

Fig. 9 presents the load-midspan deflection response from the tests together with the theoretical and design values determined using the expression given in Eq. 6. A realistic depiction of the

cracking moment is key to the accuracy of deflection calculations; therefore, the experimental cracking moment values are used herein.

It is shown in the figure that for beams B-0.61-0.24 and B-0.24-0.24, the CSA S806-12 [30] standard provides deflections that are in good agreement with the measured midspan deflections up to around 50% and 25% of the ultimate load, respectively, then underestimates the deflections at higher levels of loading. Furthermore, CSA S806-12 [30], ACI 440.1R-06 [29], and ACI 440.1R-15 [34] all underestimate the deflections for beams B-0.61-0.61 and B-0.24-0.61. ACI 440.1R-15 [34] provides deflections that are in good agreement with the measured midspan deflection up to around 60% and 50% of the ultimate load for the beams B-0.61-0.24 and B-0.24-0.24, respectively, then underestimates the deflections at higher levels of loading. ACI 440.1R-15 [34] predicts slightly higher deflections than those predicted by ACI 440.1R-06 [29], yet, both underestimate the measured midspan deflections. The method proposed by Habeeb and Ashour [23] provides deflections that are in good agreement with the measured deflections up to approximately 40% and 45% of the ultimate loading for beams B-0.61-0.24 and B-0.24-0.24, respectively, while this approach overestimates the deflections at higher levels of loading. On the other hand, this method underestimates the measured midspan deflections for the beams B-0.61-0.61 and B-0.24-0.61. However, it is noteworthy that the modification suggested by Habeeb and Ashour [23] gives a reasonable prediction to the experimental results for BFRP RC continuous beams especially at high levels of applied load.

(a)

(b)

(c)

(d)
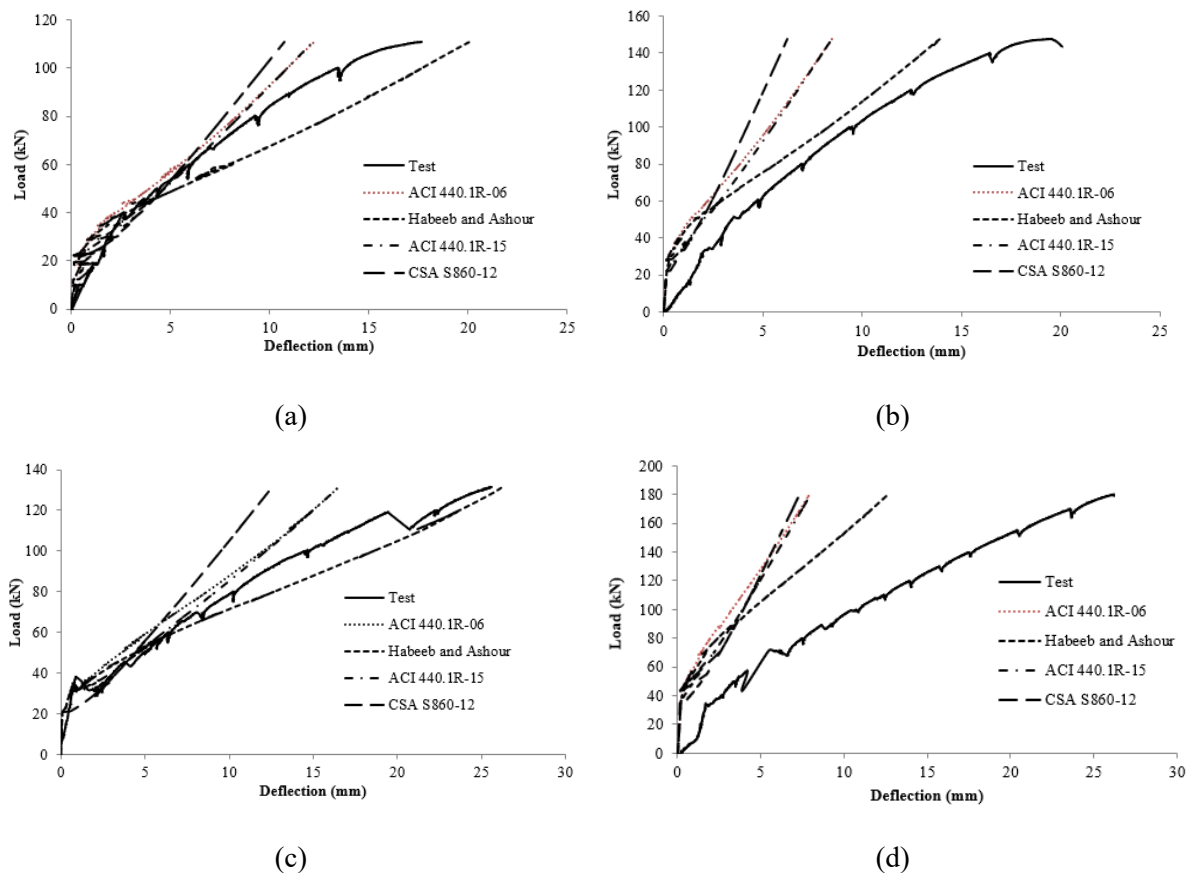
Figure 9: Experimental and predicted deflection for the beam (a) B-0.61-0.24; (b) B-0.61-0.61; (c) B-0.24-0.24 ;and (d) B-0.24-0.61

Conclusions

This paper presents the details and results from an experimental study aimed at investigating the structural performance of continuous concrete beams reinforced with BFRP rebars and stirrups. Four two-span continuous beams were tested until failure, and attention is given in the analysis to the load-deflection response, the cracking moments, the moment capacity, the moment redistributions that occurred as well as the deflections. These results are compared with the values obtained from the American and Canadian design standards for the cracking moments, moment capacities and deflections. Based on the test results and discussion presented herein, the following conclusions and recommendation are drawn:

- It is shown that beams with similar reinforcement ratios in the sagging moment regions had similar stiffnesses prior to failure. The beams with similar reinforcement ratios at the interior support exhibited comparable levels of deflection at the ultimate load. Furthermore, beams with a relatively high reinforcement ratio in the sagging moment region displayed a stiffer response, regardless of the reinforcement ratio at the interior support, resulting in relatively lower deflections overall at failure.
- For three of the four examined beams (namely B-0.61-0.24, B-0.61-0.61 and B-0.24-0.61), failure occurred due to concrete crushing in combination with diagonal tension cracks which developed at one side of the interior supports. The fourth member (B-0.24-0.24) failed due to a diagonal crack near the point of loading on the right hand span of the beam.
- The average angle of inclination of the failure plane for all tested beams was 54° to the longitudinal axis, which was steeper than observed for simply supported beams (44°).
- The failure load of the beams increased as the reinforcement ratio in the sagging moment regions increased as moments were redistributed from the hogging moment region to the sagging moment region. Hence it is recommended that a relatively high reinforcement ratio in the sagging moment region coupled with a reduced reinforcement ratio in the hogging moment region may lead to efficient and economic designs.
- Both the American and Canadian design codes tend to overestimate the cracking moments for all of the tested beams since the design guidance currently ignores the influence of reinforcement area, reinforcement stiffness, and the surface shape on the cracking moment.
- In contrast to the assumption in existing design codes that moment redistribution does not occur in BFRP RC beams, the results of the tests presented herein shows that for the range of parameters examined, at least 20% moment redistribution can be recommended in design. However, the recommended level of redistributions can be affected by many factors included the reinforcement ratio, bond properties, type of loading and boundary conditions, the cracked zone of concrete and concrete strength and shrinkage. It is suggested that these are examined in future research studies.

- The CSA S806-12 design standard yields less conservative predictions for the hogging moment capacity of the tested beams than those predicted by ACI 440.1R-06 design guideline. Furthermore, both Canadian and American design codes overestimate the sagging moment capacity.
- ACI 440.1R-06, ACI 440.1R-15 and CSA S806-12 generally underestimate the deflections for the tested beams, particularly at higher loads. The modification factor proposed by Habeeb and Ashour [23] to the ACI 440.1R-06 expressions for calculating the effective second moment of area for continuous concrete beams was shown to provide a reasonable predictions compared with the experimental results, especially in the higher loaded portion of the response, hence, it is recommended in deflection predictions.

Acknowledgements

References

[1] Apostolopoulos, C.A. and Papadakis, V.G. Consequences of steel corrosion on the ductility properties of reinforcement bar. Construction and Building Materials 2008; 22(12): 2316-2324.

[2] Ožbolt, J., Balabanić, G. and Kušter, M. 3D Numerical modelling of steel corrosion in concrete structures. Corrosion Science 2011; 53(12): 4166-4177.

[3] Frosch, R.J., Labi, S. and Sim, C. Increasing Bridge Deck Service Life: Volume I—Technical Evaluation 2014.

[4] Brik, V. Advanced concept concrete using basalt fiber/BF composite rebar reinforcement. IDEA Project 2003; 86: 71-71.

[5] Ross, A. Basalt fibers: alternative to glass?. Composites Technology 2006;12(4).

[6] Sim, J. and Park, C., Moon, D.Y. Characteristics of basalt fiber as a strengthening material for concrete structures. Composites Part B: Engineering 2005; 36(6-7): 504-512.

[7] Theriault, M. and Benmokrane, B. Effects of FRP reinforcement ratio and concrete strength on flexural behaviour of concrete beams. Journal of composites for construction 1998;2(1): 7-16.

[8] Goldston, M., Remennikov, A. and Sheikh, M.N. Experimental investigation of the behaviour of concrete beams reinforced with GFRP bars under static and impact loading. Engineering Structures, 2016;113: 220-232.

[9] Ashour, A.F. Flexural and shear capacities of concrete beams reinforced with GFRP bars. Construction and Building Materials 2006; 20(10): 1005-1015.

[10] Kaszubska, M., Kotynia, R. and Barros, J.A.,. Influence of longitudinal GFRP reinforcement ratio on shear capacity of concrete beams without stirrups. Procedia engineering 2017; 193: 361-368.

[11] Guadagnini, M., Pilakoutas, K. and Waldron, P. Shear performance of FRP reinforced concrete beams. Journal of reinforced plastics and composites 2003; 22(15): 1389-1407.

[12] Bentz, E.C., Massam, L. and Collins, M.P. Shear strength of large concrete members with FRP reinforcement. Journal of Composites for Construction 2010; 14(6): 637-646.

[13] El Ghadioui, R., Proske, T., Tran, N.L. and Graubner, C.A. Structural behaviour of CFRP reinforced concrete members under bending and shear loads. Materials and Structures 2020; 53:1-16.

[14] Shamass, R. and Cashell, K.A. Experimental investigation into the flexural behaviour of basalt FRP reinforced concrete members. Engineering Structures 2020; 220: 110950.

[15] Elgabbas, F., Vincent, P., Ahmed, E.A. and Benmokrane, B.,. Experimental testing of basalt-fiber-reinforced polymer bars in concrete beams. Composite Part B-Engineering 2016; 91: 205-218.

[16] Zhang, L., Sun, Y. and Xiong, W. Experimental study on the flexural deflections of concrete beam reinforced with Basalt FRP bars. Materials and Structures 2015; 48(10): 3279-3293.

[17] Tomlinson, D. and Fam, A. Performance of concrete beams reinforced with basalt FRP for flexure and shear. Journal of Composites for Construction 2015; 19(2): 04014036.

[18] Issa, M.A., Ovitigala, T. and Ibrahim, M. Shear behaviour of basalt fiber reinforced concrete beams with and without basalt FRP stirrups. Journal of Composites for Construction 2016; 20(4): 04015083.

[19] Jumaa, G.B. and Yousif, A.R. Size effect in shear failure of high strength concrete beams without stirrup reinforced with basalt FRP bars. KSCE Journal of Civil Engineering 2019; 23(4): 1636-1650.

[20] Jumaa, G.B. and Yousif, A.R. Size effect on the shear failure of high-strength concrete beams reinforced with basalt FRP bars and stirrups. Construction and Building Materials 2019; 209: 77-94.

[21] Duic, J., Kenno, S. and Das, S. Performance of concrete beams reinforced with basalt fibre composite rebar. Construction and Building Materials 2018; 176: 470-481.

[22] El-Mogy, M., El-Ragaby, A. and El-Salakawy, E. Flexural behaviour of continuous FRP-reinforced concrete beams. Journal of Composites for Construction 2010; 14(6): 669-680.

[23] Habeeb, M.N. and Ashour, A.F. Flexural behaviour of continuous GFRP reinforced concrete beams. Journal of composites for construction, 2008; 12(2): 115-124.

[24] Ashour A.F. and Habeeb, M.N. Continuous concrete beams reinforced with CFRP bars. Proceedings of the Institution of Civil Engineers-Structures and Buildings, 2008; 161(6): 349-357.

[25] Zhang, W., Ye, Z. and Gu, X. Effects of stirrup corrosion on shear behaviour of reinforced concrete beams. Structure and Infrastructure Engineering 2017;13(8): 1081-1092.

[26] El-Sayed, A.K., Hussain, R.R. and Shuraim, A.B.,. Influence of stirrup corrosion on shear strength of reinforced concrete slender beams. ACI Structural Journal 2016; 113(6): 1223-1232.

[27] Rahman, S.M. and El-Salakawy, E. STR-895: MOMENT REDISTRIBUTION OF GFRP-RC CONTINUOUS T-BEAMS 2016.

[28] Baša, N., Ulićević, M. and Zejak, R. Experimental research of continuous concrete beams with GFRP reinforcement. Advances in Civil Engineering 2018.

[29] American Concrete Institute. Committee 440. Guide for the Design and Construction of Concrete Reinforced with FRP Bars: ACI 440.1 R-06. Farmington Hills: American Concrete Institute, 2006.

[30] Canadian Standards Association. Design and Construction of Building Structures with Fibre-Reinforced Polymers, (CAN/CSA S806-12). Canadian Standards Association Mississauga, Ont, 2012.

[31] Mahmoud, K. and El-Salakawy, E. Shear strength of GFRP-reinforced concrete continuous beams with minimum transverse reinforcement. Journal of Composites for Construction 2014;18(1): 04013018.

[32] Mahmoud, K. and El-Salakawy, E. Effect of transverse reinforcement ratio on the shear strength of GFRP-RC continuous beams. Journal of Composites for Construction 2016; 20(1): 04015023.

[33] ISO. "Fibre-reinforced polymer (FRP) reinforcement of concrete: Test methods. Part 1: FRP bars and grids." ISO 10406-1-05, Switzerland, 2015.

[34] American Concrete Institute. Committee 440. Guide for the Design and Construction of Concrete Reinforced with FRP Bars: ACI 440.1 R-15. Farmington Hills: American Concrete Institute, 2015.

[35] American Concrete Institute. Committee 318. Building Code Requirements for Reinforced Concrete: ACI 318-08. American Concrete Institute, 2008.

[36] Branson, D. E. Deformation of Concrete Structures, McGraw-Hill, New York, 1977, 537.